Soft Matter

Packing Transitions in the Elastogranular Confinement of a Slender Loop

Journal:	*Soft Matter*
Manuscript ID	SM-ART-10-2019-002152.R1
Article Type:	Paper
Date Submitted by the Author:	07-Jan-2020
Complete List of Authors:	Schunter, Jr., David; Boston University, Mechanical Engineering Czech, Regina ; Boston University, Mechanical Engineering Holmes, Douglas; Boston University, Mechanical Engineering

Journal Name

ARTICLE TYPE

Cite this: DOI: 00.0000/xxxxxxxxxx

Packing Transitions in the Elastogranular Confinement of a Slender Loop

David J. Schunter, Jr.,*[a] Regina K. Czech,[a] and Douglas P. Holmes*[a]

Received Date
Accepted Date

DOI: 00.0000/xxxxxxxxxx

Confined thin structures are ubiquitous in nature. Spatial and length constraints have led to a number of novel packing strategies at both the micro-scale, as when DNA packages inside a capsid, and the macro-scale, seen in plant root development and the arrangement of the human intestinal tract. Here, we investigate the resulting packing behaviors between a growing slender structure constrained by deformable boundaries. Experimentally, we vary the arc length of an elastic loop injected into an array of soft, spherical grains at various initial number densities. At low initial packing fractions, the elastic loop deforms as though it were hitting a flat surface by periodically folding into the array. Above a critical packing fraction ϕ_c, local re-orientations within the granular medium create an effectively curved surface leading to the emergence of a distinct circular packing morphology. These results bring new insights into the packing behavior of wires and thin sheets, and will be relevant to modeling plant root morphogenesis, burrowing and locomotive strategies of vertebrates & invertebrates, and developing smart, steerable needles.

Under rigid confinement, thin structures tend to adopt the geometry circumscribed by their confining boundaries[1–5]. Draping a thin sheet or filament onto a rigid flat surface causes it to fold[6,7], leading to the formation of multiple alternating loops as the arc length is continuously increased[8,9]. In the presence of a rigid curved surface, flexible structures may coil, roll-up, or spiral, as seen in the packaging of household paper products[10] or when pulling a thin sheet through a small aperture[11]. Similar folding and circular morphologies have also been observed in thin structures under flexible/soft constraints[12,13]. In both types of confinement, the material and structural characteristics of the containing space (geometry, rigidity, etc.) are effectively fixed: even when softly confined, packing thin structures can only slightly influence their flexible containers[14]. What happens when the notions of boundary compliance and geometry are less clearly defined is not well understood, yet this situation frequently occurs when slender objects pack within complex and fragile media.

Drawing inspiration from growth patterns in *Arabidopsis* roots [Fig. 1(vi), 1(VI)][15–18] and previous work on the buckling of thin rods in granular media[19–22], we consider the packing of an elongating slender loop within a 2D granular bed, where we observe the same packing transitions and geometries. In this Letter, using a combination of experiments and scaling analysis, we characterize the emergent behavior of these distinct packing morphologies, and the role played by the evolution of the surrounding granular medium. These elastogranular systems will be helpful in the study of piercing & penetration at soft-solid interfaces[23,24], in the design of dirigible surgical tools[25], and provide a novel approach for looking at the packing of thin elastic structures across a spectrum of confinement strengths[14,22,26,27].

Experimentally, we increased the arc length of an elastic loop within a container filled with a monolayer of grains ‡. The granular monolayers were prepared with initial packing fractions ϕ_0, and consisted of soft, spherical hydrogel grains (MagicWater-Beads) of radius $r = 9.28 \pm 0.164$ mm that were randomly placed in the experimental enclosure (length $L = 279.4$ mm, and width $W = 438.15$ mm) [Fig. 1]. A long strip of polyethylene terephthalate (PET) film, identical to that used in reel-to-reel cinema projection, is clamped within a custom-built film sprocket/roller mount to form a “pinched" elastic loop[28,29] with initial arc length $S_0 \approx 75$ mm, width $b = 35$ mm (out of the page in Fig. 1), and thickness $h = 0.138$ mm [Figs. 1(i), 1(I)]. This device creates a single clamped-roller boundary condition allowing for incremental adjustments Δ to the loop's arc length to a new current length $S = S_0 + \Delta$, and up to a maximum value $S/S_t = 1$ (where the film's linear length $S_t = 2435.2$ mm; see videos S1 & S2)§.

[a] *Mechanical Engineering, Boston University, Boston, MA, 02215, USA*
*djsj@bu.edu; dpholmes@bu.edu

† *Electronic Supplementary Information (ESI) available: [details of any supplementary information available should be included here]. See DOI: 00.0000/00000000.*

‡ Very similar deformations and packing transitions were observed when an elastic strip with a free boundary was inserted into a granular array, however the elastic loop removes any complications with how and where the free edge of the elastica finds the edge of the container.

§ An Arduino with stepper-motor stack (powering two Nema-17 steppers) allows us to smoothly control the injected arc length Δ. Each film sprocket is mounted atop the

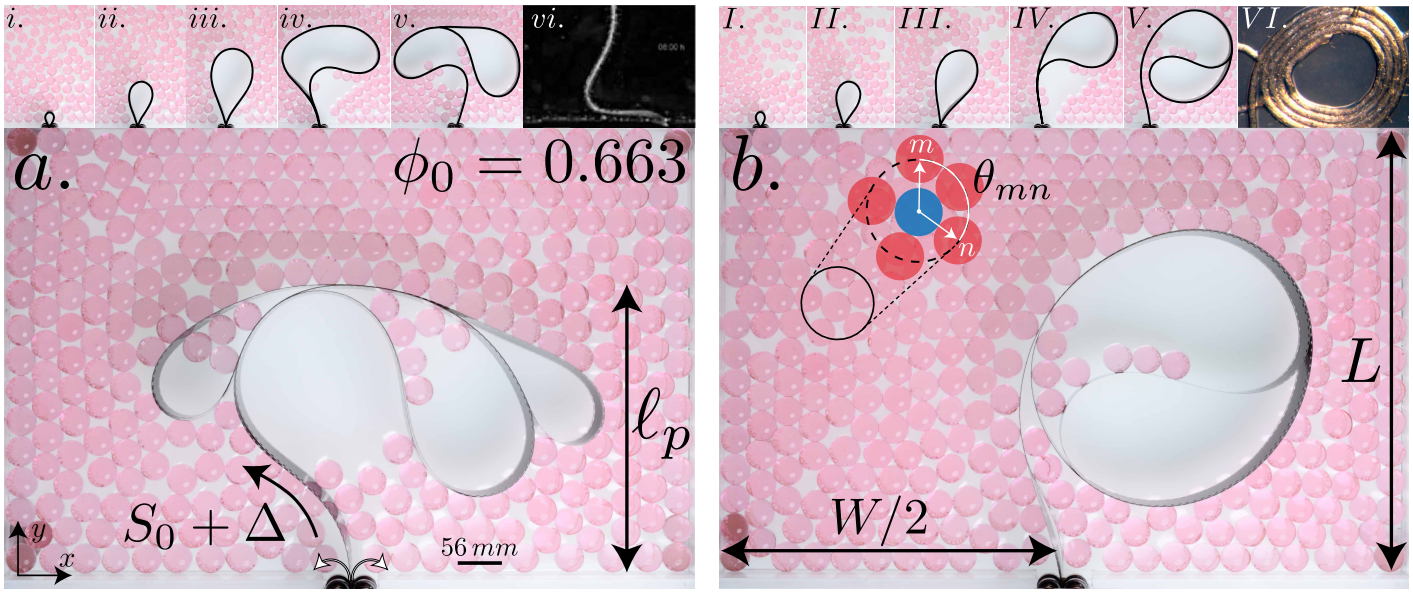

Fig. 1 A slender elastic loop elongating into granular arrays at varying initial packing fraction ϕ_0. (a) Below a critical initial packing fraction $(\phi_0 < 0.641)$, the elastic loop will pack into the granular medium by adopting a characteristic folded geometry. (b) For $\phi_0 \geq 0.641$, a characteristic circular packing morphology emerges. **Inset:** Inter-particle angle and center-to-center distances used to define orientational order. **Sequences:** At low values of injected arc length, the two morphologies appear the same, where $\Delta/S_t \approx \{0.03, 0.06, 0.12\}$ in frames (i,I), (ii,II), (iii,III) respectively. As the arc length continues to increase [$\Delta/S_t \approx \{0.23, 0.46\}$ in (iv,IV), (v,V)], distinct packing strategies for the thin loop begin developing. Once set, the resulting circular and folded morphologies bear a striking resemblance to developing *Aribidopsis* roots in contact with a hard agar substrate (vi,VI) [Adapted from [15,16]].

As the arc length increases by a small amount Δ at a quasistatic rate of 2.2 mm/s, the elastic loop maintains its characteristic racket shape, a geometry observed over a wide range of length scales in fluid-thin structure interactions[30,31] [Figs. 1(i-ii), 1(I-II)]. In the absence of any externally applied forces, the left-right symmetry of this configuration hypothetically persists in the limit $\Delta \gg 1$, however, the presence of the granular medium acts to confine and buckle the elastic loop. Thin structures favor bending over stretching as a deformation response to applied forces; indeed at larger Δ-values, the symmetry of the pinched-loop configuration is lost as the thin structure relaxes stored curvature (housed primarily in the distal tip region) [Figs. 1(iv), 1(IV)]. Continued increase of the arc length [Figs. 1(v), 1(V)], along with local re-arrangements in the granular medium [Fig. 2], elicit one of two distinct packing morphologies in the elastic loop: a disordered *folded* phase [Fig. 1(a)] observable over the entire range of initial packing fractions, $0 \leq \phi_0 \leq 0.828$, and an ordered *circular* phase [Fig. 1(b)] emerging only in higher density arrays above a critical initial packing fraction $\phi_c = 0.641$¶. (Our terminology is chosen to maintain consistency with previous works on the packing of flexible structures in both rigid and flexible confinement[1,11,13,14,32–35]).

The implication here is that once jammed, the granular medium acts like a container, housing the loop with a certain

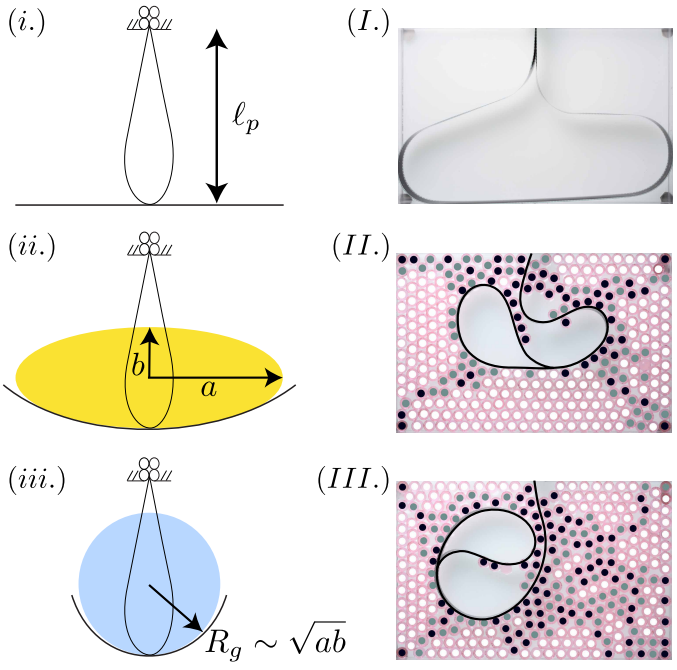

Fig. 2 The role of the granular contour. While a freely injected elastic loop (i) will drape against a flat surface (I), the introduction of the granular medium can modify the curvature (ii,iii) and rigidity (II,III) of the surface against which the loop deforms. The influence of local bond orientation order ψ^6, which provides a measure of confining boundary rigidity, is apparent in both (II) folded and (III) circular packing morphologies. (○) $\psi^6 \geq 0.66$; (◉) $0.33 < \psi^6 < 0.66$; (●) $\psi^6 \leq 0.33$. The experiments shown in (I-III) are at the same injected arc length ($\Delta/S_t \approx 0.46$).

driveshaft of its own stepper motor. Small teeth, circling the upper and lower rim of each film sprocket, grip the edges of the 35-mm film. As the sprockets begin turning with a synchronized rotational velocity [white arrows, bottom Fig. 1(a)], the loop starts lengthening.

¶ When $\phi_0 \geq 0.774$, a clear acrylic lid is placed over the enclosure to prevent sections of the loop from dislodging vertically out of the monolayer at larger Δ-values.

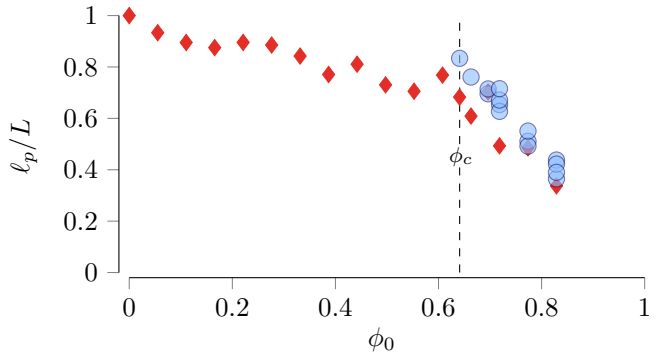

Fig. 3 Penetration depth ℓ_p normalized by the length L of the experimental enclosure, as a function of initial packing fraction ϕ_0 for folding (red diamonds) and circular (light blue circles) geometries.

level of rigidity and degree of boundary curvature (ranging from flat to semi-circular) that drives the system to adopt one morphology over the other. Looking at the local orientational order $\psi^6 = \left\langle N_b^{-1} \sum_{n=1}^{N_b} e^{6i\theta_{mn}} \right\rangle$ [inset, Fig. 1(b)], which measures the degree to which a local granular neighborhood of monodisperse grains are hexagonally arranged[36], provides a visual and quantifiable means of assessing rigidity in a given array: highly-ordered regions (*i.e.* $\psi^6 \geq 0.66$) act like a nearly rigid wall of grains against which the elastic loop deforms [Figs. 2(II), 2(III); videos S6 & S7]. Determining the extent to which the surrounding grains form a curved surface is more subtle and requires looking at how elastic deformations in the loop influence the formation of these boundaries.

We begin by quantifying the spatial extent of the slender loop's deformation via a penetration depth ℓ_p, the maximum distance (in the y-direction in Fig. 1) which the thin structure can deform into an array at a given ϕ_0, and a radius of gyration R_g, characterizing the (general) area within which elastic deformations localize. The measurement of penetration depth is straightforward and progressively larger ϕ_0-values are seen to result in lower values of ℓ_p overall, regardless of the thin structure's chosen morphology [Fig. 3]. The intuitive result that it becomes increasingly difficult to introduce additional arc length into a decreasing amount of available surface area, contrasts with the behavior observed above ϕ_c, in which the circular morphology arises as a deformation mode. At equal ϕ_0, penetration depths for circular packing are always greater than or equal to ℓ_p-values measured in folded packing configurations [Fig. 3]. This behavior suggests that circular packing may be energetically preferable for thin structures elongating within dense granular media ($\phi_0 > \phi_c$) in finite domains, commonly observed in root-bound plants in need of re-potting[37].

Values of ℓ_p remain nearly constant (at their maximum value) after the initial buckling of the loop, however, inklings of the final morphology only become apparent well into the post-buckling regime [Figs. 1(v), 1(V)]: the loop continues to pack into the grains, further densifying the surrounding granular network. We quantify the evolution of the surrounding medium towards a curved/circular profile by defining a radius of gyration R_g. Recall that the area of an ellipse (with semi-major/semi-minor axis' $\{a,b\}$) $A_e = \pi ab$, is equivalent to a circular area $A_c = \pi R_g^2$, whose radius we take as defining the radius of gyration R_g. This approach allows us to measure R_g in all experiments, as the elongating loop tends to accumulate in elliptically-bounded regions below ϕ_c and in folded configurations [Fig. 2(ii)]. Balancing terms between $\{A_e, A_c\}$ shows that the radius of gyration: $R_g \sim \sqrt{ab}$ (where for circular morphologies $a = b$) [Fig. 2(iii)].

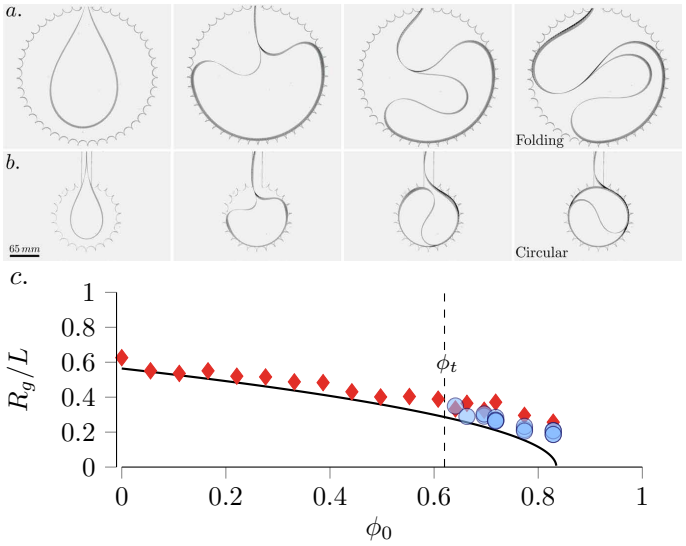

Fig. 4 (a) Injection of an elastic loop into a rigid container with $R = 117.78$ mm leads to periodic folding, while (b) injection into a container with $R = 54.51$ mm leads to circular packing. The walls were cut with periodic rounded features to reduce the contact area, and thus the friction, between the loop and the wall. (c) Radius of gyration R_g, normalized by the length L of the experimental enclosure, as a function of initial packing fraction ϕ_0 for folding (red diamonds) and circular (light blue circles) geometries. The scaling (**2**) (solid black line) yields a critical initial packing fraction $\phi_t = 0.621$.

Measuring R_g over the range of ϕ_0-values (using the freely-available ImageJ platform[38]), we observe that for granular arrays prepared at low to mid-range packing fractions, $\phi_0 \lesssim 0.6$, the elastic loop exclusively adopts a folded geometry. In this regime the slender structure is only weakly confined[14]. This behavior persists up until a critical packing fraction $\phi_c = 0.641$, where we begin to see the emergence of the circular morphology. This does not imply that we always observe circular packing for $\phi_0 \geq \phi_c$, only that conditions within the system are now favorable for its emergence. The absence of the circular morphology at lower initial packing fractions reinforces the argument made previously with ψ^6 that a certain strength of confinement (*i.e.* level of rigidity) is needed by the grains to observe circular packing: the grains must be able to form and maintain a semi-circular boundary contour against which the elastic loop deforms.

We speculate that the confining geometry necessary for the transition between folded and circular patterns is defined by a critical radius of gyration R_c. Given a 2D array of grains with packing fraction $\phi_0 \geq \phi_c$, R_c is the circular inclusion that would cause the array to jam locally, forming an effectively rigid containing space within which the slender loop will pack. It was previously found[19] that the soft hydrogel grains used in these experiments become jammed at a critical packing fraction $\phi_j =$

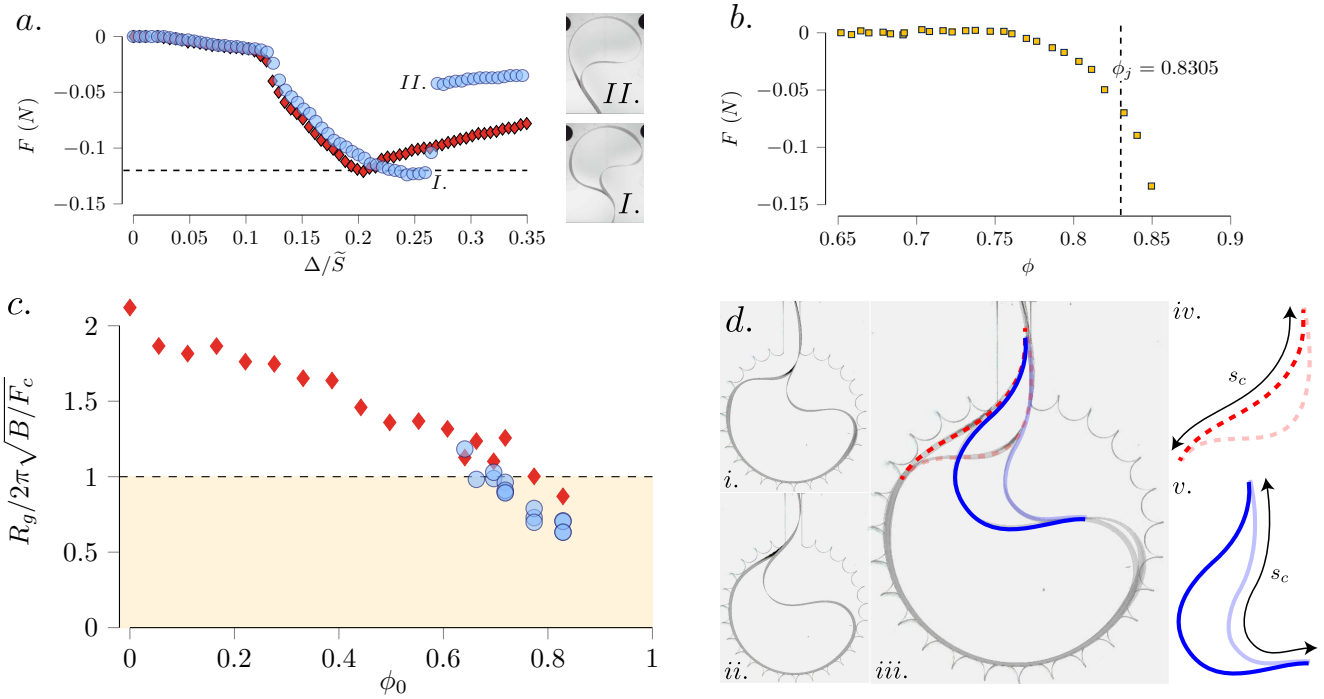

Fig. 5 (a) An elastic loop, lengthening into a semi-circular rigid container with $R = 54.95$ mm, buckles at a critical force F_c in both folded (red diamonds) and circular (light blue circles) configurations. Throughout the loading path (when $S \geq \tilde{S} =$ arc length at contact with rigid boundary), force values span the same range as the reaction forces (b) generated in a compressed granular array as $\phi \to \phi_j$ [19]. (c) Rescaling the radius of gyration R_g by the critical length $L_c = 2\pi\sqrt{B/F_c}$ eliminates system size dependence. Notably, circular packing emerges when R_g and L_c are of the same order-of-magnitude (shaded region). (d) Images of the elastic loop *i.* just prior to buckling and *ii.* immediately following buckling. *iii.* Images from *i.* and *ii.* overlaid on each other, with the two regions of the loop that appear to buckle highlighted (dashed red; solid blue). The length of the *iv.* left and *v.* right half of the loop that appears to buckle are labeled s_c. Both labeled arc lengths are longer than $2R_g$, meaning this structure will pack with a circular morphology.

0.8305 ± 0.0135. As Δ increases in the limit that $\phi \to \phi_j$, the total surface area (available to the grains) within the array will change by an amount proportional to a circular area $\sim \pi R_c^2$, such that: $\phi_j \sim N\pi r^2/(LW - \pi R_c^2)$‖. Rearranging to isolate for R_c yields the scaling for the critical radius of gyration as:

$$R_c \sim \sqrt{\left(\frac{LW}{\pi}\right) - \left(\frac{Nr^2}{\phi_j}\right)}. \quad (1)$$

The RHS of Eq. (**1**) is composed entirely of known values, which yields $R_c \simeq 94.32$ mm. We corroborate this scaling argument by performing a set of additional "toy model" experiments where the elastic loop is injected into circular, rigid walled confinements of different sized internal diameters. This has the effect of removing the granular part of the problem and creates a truly rigid confining boundary with which we can test our initial assumption of treating the jammed grains as a rigid, curved surface above ϕ_c [Figs. 4(a)-4(b); videos S3 & S4]. Experiments using this toy model produce a value for the critical radius of gyration $R_t \simeq 99.19$ mm, close to the value obtained using the scaling in Eq. (**1**).

Although the grains are absent in the toy model experiments, we can still infer hypothetical values of ϕ_0 associated with each R_g tested for these idealized rigid boundaries. A simple rewriting of Eq. (**1**) yields the hypothetical ϕ_0-value for a particular rigid circular confinement region found in the toy model experiments as:

$$\phi_0 \sim \phi_j \left(1 - \frac{\pi R_g^2}{LW}\right). \quad (2)$$

Rearranging to isolate for R_g/L, Eq. (**2**) is plotted as a solid black line in Fig. 4(c), alongside experimental measurements for both folded (red diamonds) and circular (light blue circles) runs. The scaling (**2**) is in very good agreement with experiments; it validates R_g as a measure of system physics and provides a lower bound to the experimental data expressing the provisional/nominal system size [14].

Normalizing R_g by an arbitrary system dimension creates *de facto* system-size dependence; ideally, we want to be able to describe these elastogranular interactions in a scale-invariant way. As a length scale of granular origin, R_g can be regarded as a proxy for the geometric constraints a given grain configuration imposes on the slender loop. The coupling between buckling in the thin loop structure and the evolution of its granular containing space depends on elasticity of the loop. Drawing on similarities with other physical systems involving slender structures [7,31,39–41], we expect that a characteristic length scale will play an important role in this coupled system.

Given the negligible effects of stretching and the fact that the film's width is much smaller than its length ($b \ll S$), we can invoke the so-called "thin strip limit" [42], in which the plate equations nor-

‖ We can account for the surface area of the film by either ignoring it in the limit $h \ll 1$, a safe assumption here, or considering it as being included in the measurement of R_g.

mally needed to describe this problem become analogous to the equations for thin rods. Therefore, the slender loop can then be treated as an Euler column, where buckling occurs when S is increased to a critical length L_c, such that[42]:

$$L_c = 2\pi\sqrt{B/F_c}. \tag{3}$$

The bending rigidity $B = EI$ of the slender loop (with Young's modulus E and second moment of area $I = h^3 b/12$) is calculated using the "free-fold test" via the formula: $B = 1.342\mu\delta^3$ (where μ is the weight per unit length and δ is the height of the loop when laying/placed on its side)[43]. The result, $B = 20.70$ N·mm^2, compares quite well with that obtained using material parameters for PET commonly cited in the literature[44], $B = 21.46$ N·mm^2. Using the toy-model experiments, we directly measured the critical buckling force F_c for the idealized case of a truly rigid confining boundary. We observe a buckling force of $F_c \approx -0.12$ N for both folded [red diamonds; Fig. 5(a)] and circular [light blue circles; Fig. 5(a)] packing morphologies. We independently compared this value to the reaction force of the grains measured as the size of the container was decreased[19], *i.e.* as ϕ is increased. The critical buckling force of the elastic loop is proportional to the reaction force measured at or just above the jamming point ϕ_j for these particular grains, where an effectively rigid, locally jammed region of the granular boundary generates a reaction force [Fig. 5(b)].

Fig. 5(c) shows R_g as a function of ϕ_0, where R_g has been rescaled by the critical length $L_c = 82.52$ mm. Circular packing necessitates buckling of the slender loop (allowing it to accommodate excess length or "buffer-by-buckling"[45]) and the presence of a circular confining boundary, conditions which become possible when R_g and L_c are of equal orders-of-magnitude:

$$R_g = R_c \sim L_c\,. \tag{4}$$

The existence of this length scale helps illuminate the lack of physical information provided by the penetration depth: L_c is the length scale of elastic buckling. While we calculate L_c from independent measurements of B and F_c, a natural question is: what length of the elastic loop does L_c correspond to? Returning to the toy model experiments, we isolate two images of the elastic loop just prior to buckling [Fig. 5(d)–i.] and just after buckling [Fig. 5(d)–ii.] Overlaying these images [Fig. 5(d)–iii.], we identify two portions of the elastic loop that appear to buckle at the same time (one on the left half of the loop, the other on the right half). Isolating each length that appears to buckle, and labeling it s_c, we would expect these structures to pack with a circular morphology if we take $L_c \equiv s_c/2$ and find that $s_c/2 \gtrapprox R_g$. We find that both lengths are approximately greater than or equal to the radius of gyration containing the loop ($R_g = 67.2$ mm; $s_c/2 = 66.9$ mm [dashed red], $s_c/2 = 70.6$ mm [solid blue]), which suggests these lengths that appear to buckle are what drives the selection of the packing morphology**.

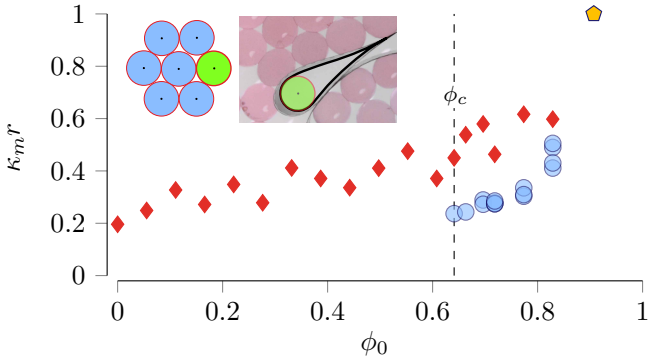

Fig. 6 Normalized maximum measured curvature κ_m as a function of initial packing fraction ϕ_0 for folding (red diamonds) and circular (light blue circles) geometries. The yellow pentagon represents the anticipated limiting behavior of this elastogranular system **Inset:** As $\phi_0 \to 0.907$, the maximum observable loop-tip curvature will approach a limiting value κ_h, with a radius of curvature on the order of the average size grain radius in an array.

In circular morphologies, the energy minimization strategy for the elastic loop is essentially fixed once the circular profile is formed. Additional injected arc length will wrap around this inner circle similar to DNA spooling within a capsid[46]. We can measure this radius value experimentally, or infer a value using the scaling in (**1**). In folded morphologies, we observe the formation of a cascade of loops increasing in number as either Δ or ϕ_0 become larger, with loop-tip curvature values appearing to approach a limiting value κ_h. A similar situation has been observed numerically in elastic rings with self contact[47]. The limiting curvature κ_h is the largest amount the loop may be bent by the granular medium without inducing any plastic deformation. Due to the monodispersity of the grains, we know *a priori* the granular medium will approach a hexagonal-packing configuration as an equilibrium geometry[48,49]. We thus anticipate that a loop-tip has a limiting radius of curvature, $1/\kappa_h$, on the order of the average size grain radius r [inset, Fig. 6].

Along with material considerations, how slender structures deform depends intimately on their boundary interactions. For the canonical case of elongating thin objects confined within rigid containers, the geometry, stiffness, and boundary continuity of the confining space can each contribute to the deformation morphologies adopted by these objects. By studying elastogranular packing, we are able to probe a system in which large elastic deformations occur within transitional boundaries. The discrete, flexible network of the granular medium surrounding the loop (at low packing fractions) will change under increasing confinement, becoming more analogous to a continuous, rigid containing space. Simple experimental systems such as these provide a novel investigative tool for looking at how macroscale geometric

** The transition between periodic folding and circular packing occurs when $R_g/L_c \lesssim 1$. However, the curvature near the elastic loop is dictated by the local arrangement of grains. If the grains pack with a large radius of curvature, the loop will pack periodically, even if $R_g/L_c \lesssim 1$. To confirm this using our toy model, we injected an elastic loop into an ellipse of $R_g = 67.2$ mm [see video S5], and find that it folds periodically even though packing into a circular profile with equal $R_g = 67.2$ mm led to circular packing [Fig. 4; video S4].

features can arise in complex media, and how these features in turn affect interactions with inclusions.

Conflicts of interest

There are no conflicts to declare.

Acknowledgements

The authors wish to thank Rinik Kumar for performing preliminary experiments on the free-boundary elastica. We are grateful for financial support from the National Science Foundation CMMI–CAREER through Mechanics of Materials and Structures (No. 1454153).

Notes and references

1 N. Stoop, F. K. Wittel and H. J. Herrmann, *Phys. Rev. Lett.*, 2008, **101**, 094101.
2 J. Hure, B. Roman and J. Bico, *Phys. Rev. Lett.*, 2012, **109**, 054302.
3 J. D. Paulsen, *Annual Review of Condensed Matter Physics*, 2019.
4 B. Davidovitch, Y. Sun and G. M. Grason, *Proc. Natl. Acad. Sci. U.S.A.*, 2019, **116**, 1483–1488.
5 E. Cerda, L. Mahadevan and J. M. Pasini, *Proc. Natl. Acad. Sci. U.S.A.*, 2004, **101**, 1806–1810.
6 N. M. Ribe, *Phys. Rev. E*, 2003, **68**, 036305.
7 T. G. Sano, T. Yamaguchi and H. Wada, *Phys. Rev. Lett.*, 2017, **118**, 178001.
8 D. Lloyd, W. Shanahan and M. Konopasek, *International Journal of Mechanical Sciences*, 1978, **20**, 521–527.
9 L. Mahadevan and J. B. Keller, *Siam Review*, 1999, **41**, 115–131.
10 V. Romero, E. Cerda, T. Witten and T. Liang, *Journal of Physics D: Applied Physics*, 2008, **41**, 132003.
11 L. Boué, M. Adda-Bedia, A. Boudaoud, D. Cassani, Y. Couder, A. Eddi and M. Trejo, *Phys. Rev. Lett.*, 2006, **97**, 166104.
12 R. Vetter, F. K. Wittel and H. J. Herrmann, *EPL (Europhysics Letters)*, 2015, **112**, 44003.
13 M. R. Shaebani, J. Najafi, A. Farnudi, D. Bonn and M. Habibi, *Nature Communications*, 2017, **8**, 15568.
14 R. Vetter, F. K. Wittel and H. J. Herrmann, *Nature Communications*, 2014, **5**, 4437.
15 E. Kolb, V. Legue and M.-B. Bogeat-Triboulot, *Physical Biology*, 2017.
16 F. Migliaccio and S. Piconese, *Trends in Plant Science*, 2001, **6**, 561–565.
17 F. Migliaccio, P. Tassone and A. Fortunati, *American Journal of Botany*, 2013, **100**, 4–13.
18 M. V. Thompson and N. M. Holbrook, *Plant Physiology*, 2004, **135**, 1822–1837.
19 D. J. Schunter Jr, M. Brandenbourger, S. Perriseau and D. P. Holmes, *Phys. Rev. Lett.*, 2018, **120**, 078002.
20 N. Algarra, P. G. Karagiannopoulos, A. Lazarus, D. Vandembroucq and E. Kolb, *Phys. Rev. E*, 2018, **97**, 022901.
21 A. R. Mojdehi, B. Tavakol, W. Royston, D. A. Dillard and D. P. Holmes, *Extreme Mechanics Letters*, 2016, **9**, 237–244.
22 D. J. Schunter, M. Boucher and D. P. Holmes, *Granular Matter*, 2020, **22**, 3.
23 V. Choumet, T. Attout, L. Chartier, H. Khun, J. Sautereau, A. Robbe-Vincent, P. Brey, M. Huerre and O. Bain, *PLoS One*, 2012, **7**, e50464.
24 U. Cerkvenik, B. van de Straat, S. W. Gussekloo and J. L. van Leeuwen, *Proc. Natl. Acad. Sci. U.S.A.*, 2017, **114**, E7822–E7831.
25 P. J. Swaney, J. Burgner, H. B. Gilbert and R. J. Webster, *IEEE Transactions on Biomedical Engineering*, 2012, **60**, 906–909.
26 P. Chaudhuri, L. Berthier and S. Sastry, *Phys. Rev. Lett.*, 2010, **104**, 165701.
27 F. Gosselin, P. Neetzow and M. Paak, *Phys. Rev. E*, 2014, **90**, 052718.
28 G. Domokos, W. Fraser and I. Szeberényi, *Physica D: Nonlinear Phenomena*, 2003, **185**, 67–77.
29 S. Santillan, L. Virgin and R. Plaut, *Journal of Sound and Vibration*, 2005, **288**, 81–90.
30 C. Py, P. Reverdy, L. Doppler, J. Bico, B. Roman and C. N. Baroud, *Phys. Rev. Lett.*, 2007, **98**, 156103.
31 A. E. Cohen and L. Mahadevan, *Proc. Natl. Acad. Sci. U.S.A.*, 2003, **100**, 12141–12146.
32 C. C. Donato, M. A. Gomes and R. E. de Souza, *Phys. Rev. E*, 2002, **66**, 015102.
33 M. Pineirua, M. Adda-Bedia and S. Moulinet, *EPL (Europhysics Letters)*, 2013, **104**, 14005.
34 E. Katzav, M. Adda-Bedia and A. Boudaoud, *Proc. Natl. Acad. Sci. U.S.A.*, 2006, **103**, 18900–18904.
35 N. Stoop, J. Najafi, F. K. Wittel, M. Habibi and H. Herrmann, *Phys. Rev. Lett.*, 2011, **106**, 214102.
36 N. D. Mermin, *Phys. Rev.*, 1968, **176**, 250.
37 G. Amoroso, P. Frangi, R. Piatti, F. Ferrini, A. Fini and M. Faoro, *HortScience*, 2010, **45**, 1824–1829.
38 W. S. Rasband, *http://imagej.nih.gov/ij/*, 2011.
39 C.-Y. Wang, *Journal of Applied Mechanics*, 1981, **48**, 199–200.
40 S. Mora, T. Phou, J.-M. Fromental, B. Audoly and Y. Pomeau, *Phys. Rev. E*, 2012, **86**, 026119.
41 J. Bico, É. Reyssat and B. Roman, *Annual Review of Fluid Mechanics*, 2018, **50**, 629–659.
42 B. Audoly and Y. Pomeau, *Elasticity and Geometry: from hair curls to the non-linear response of shells*, Oxford University Press, 2010.
43 R. H. Plaut, *Textile Research Journal*, 2015, **85**, 884–894.
44 *http://www.goodfellow.com/E/Polyethylene-terephthalate.html*, 2020.
45 D. Vella, *Nature Reviews Physics*, 2019, 1.
46 R. Phillips, J. Kondev, J. Theriot and H. Garcia, *Physical Biology of the Cell*, Garland Science, 2012.
47 J. E. Flaherty, J. B. Keller and S. Rubinow, *SIAM Journal on Applied Mathematics*, 1972, **23**, 446–455.
48 M. Van Hecke, *J. Phys. Condens. Matter*, 2009, **22**, 033101.
49 T. Curk, J. D. Farrell, J. Dobnikar and R. Podgornik, *Phys. Rev. Lett.*, 2019, **123**, 047801.

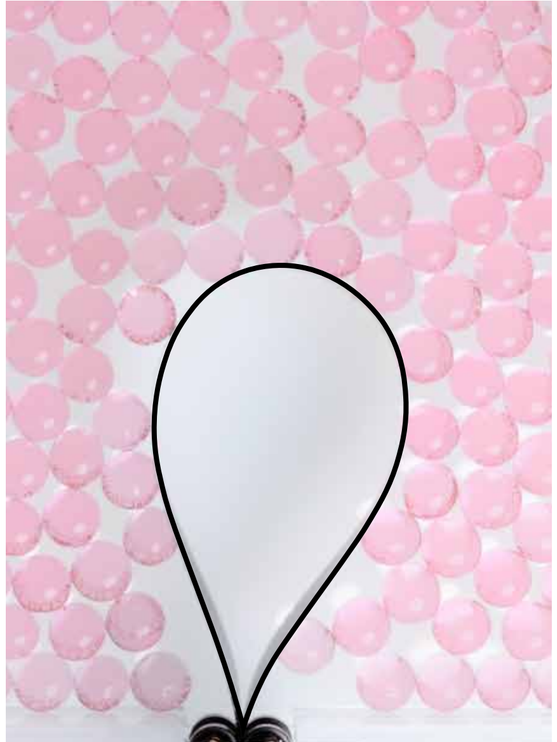

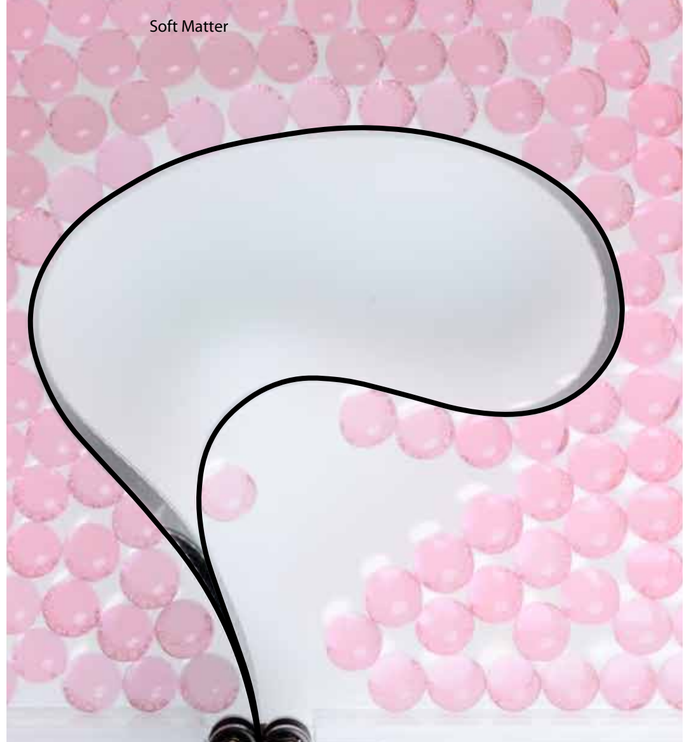

An elastic loop, lengthening in a 2D granular array, will buckle into a characteristic folded or circular packing morphology.